·Article·
Advances in Polar Science
doi: 10.3724/SP.J.1085.2013.00296
December 2013 Vol. 24 No. 4: 296-314

Global distributions of storm-time ionospheric currents as seen in geomagnetic field variations

Atsuki Shinbori[1*], Tomoaki Hori[2], Yoshimasa Tanaka[3], Yukinobu Koyama[4], Takashi Kikuchi[1,2] & Tsutomu Nagatsuma[5]

[1] Research Institute for Sustainable Humanosphere, Gokasho, Uji, Kyoto 611-0011, Japan;
[2] Solar-Terrestrial Environment Laboratory, Nagoya University, Furou-cho, Chikusa-ku, Nagoya, Aichi 464-8614, Japan;
[3] National Institute of Polar Research, 10-3 Midori-cho, Tachikawa, Tokyo 190-8518, Japan;
[4] Data Analysis Center for Geomagnetism and Space Magnetism, Graduate School of Science, Kyoto University, Kitashirakawa-Oiwake Cho, Sakyo-ku, Kyoto 606-8502, Japan;
[5] National Institute of Information and Communications Technology, 4-2-1, Nukuikitamachi, Koganei, Tokyo 184-0015, Japan

Received 30 May 2013; accepted 30 October 2013

Abstract To investigate temporal and spatial evolution of global geomagnetic field variations from high-latitude to the equator during geomagnetic storms, we analyzed ground geomagnetic field disturbances from high latitudes to the magnetic equator. The daytime ionospheric equivalent current during the storm main phase showed that twin-vortex ionospheric currents driven by the Region 1 field-aligned currents (R1 FACs) are intensified significantly and expand to the low-latitude region of ~30° magnetic latitude. Centers of the currents were located around 70° and 65° in the morning and afternoon, respectively. Corresponding to intensification of the R1 FACs, an enhancement of the eastward/westward equatorial electrojet occurred at the daytime/nighttime dip equator. This signature suggests that the enhanced convection electric field penetrates to both the daytime and nighttime equator. During the recovery phase, the daytime equivalent current showed that two new pairs of twin vortices, which are different from two-cell ionospheric currents driven by the R1 FACs, appear in the polar cap and mid latitude. The former led to enhanced northward B_z (NBZ) FACs driven by lobe reconnection tailward of the cusps, owing to the northward interplanetary magnetic field (IMF). The latter was generated by enhanced Region 2 field-aligned currents (R2 FACs). Associated with these magnetic field variations in the mid-latitudes and polar cap, the equatorial magnetic field variation showed a strongly negative signature, produced by the westward equatorial electrojet current caused by the dusk-to-dawn electric field.

Keywords **solar wind, interplanetary magnetic field, geomagnetic storm, convection electric field, field-aligned currents, equatorial electrojet, NBZ FAC system**

Citation: Shinbori A, Hori T, Tanaka Y, et al. Global distributions of storm-time ionospheric currents as seen in geomagnetic field variations. Adv Polar Sci, 2013, 24:296-314, doi: 10.3724/SP.J.1085.2013.00296

1 Introduction

It is well known that the large-scale convection electric field generated in the magnetosphere via merging of the interplanetary magnetic field (IMF) and earth's magnetic field leads to worldwide ionospheric currents responsible for DP 2 (disturbance of polar field 2) magnetic field variations, both in the high-latitude region and at the dayside geomagnetic dip equator[1-2]. Using high time-resolution magnetometer data, Kikuchi et al.[3] showed that the large-scale convection electric field is transmitted from high latitudes to the dip equator instantaneously within 25 s. This instantaneous transmission is explained by zero-order transverse magnetic (TM0) mode waves in the earth-ionosphere waveguide[4-5]. Kikuchi et al.[3] verified that DP 2 variations at auroral latitudes are caused by ionospheric

* Corresponding author (email: shinbori@rish.kyoto-u.ac.jp)

Hall currents, based on data analysis of the European incoherent scatter (EISCAT) radar and magnetometer chain; the dayside equatorial DP 2 variations are caused by ionospheric Pedersen currents enhanced by the Cowling effect[6-7]. Similar DP2-type ionospheric currents can be applied to geomagnetic perturbations such as geomagnetic sudden commencements (SCs)[8-10], global Pc 5 pulsations[11], substorm growth phases[12-14], and geomagnetic storms[15-17].

The enhanced dawn-to-dusk convection electric field during geomagnetic storms carries hot plasma of the plasma sheet from the near-earth magnetotail into the inner magnetosphere, which causes a partial ring current (PRC) under the action of the gradient and curvature drifts. The PRC in the inner magnetosphere enhances Region 2 field-aligned currents (R2 FACs) flowing into and out of the ionosphere in the afternoon and morning sectors, respectively. The shielding electric field is built up in the mid-latitude ionosphere, associated with development of the R2 FACs[17-22]. The direction of this field is opposite to that of the convection electric field in the inner region of the ring current/plasma sheet and middle to equatorial latitude ionosphere. During the southward IMF, the convection electric field develops and exceeds the shielding electric field in the low-latitude and equatorial ionosphere (i.e., undershielding condition). The shielding electric field develops after growth of the convection electric field, and becomes effective in 15–20 min as inferred from ground magnetometer observations[14,23], and in 20–30 min from theoretical calculations[22,24]. The enhanced shielding electric field often causes reversed electric fields in mid and low latitudes when the convection electric field decreases abruptly owing to the northward turning of the IMF[25-28]. The reversed electric field was identified as the overshielding electric field[26-28] and the reversed ionospheric current appears at the equator as the equatorial counter electrojet (CEJ)[14,17,25,29-31]. According to model calculations, the overshielding electric field lasts for several tens of minutes[24, 32].

Wilson et al.[15] demonstrated intensified DP 2 currents at mid-latitudes (Fredricksburg at 49.1 magnetic latitude and Memanbetsu at 34.6) and high latitudes during the initial and main phases of a major magnetic storm, when the Combined Release and Radiation Effects Satellite (CRRES) observed a significant electric field inside the ring current. The authors pointed out that the ionospheric electric field responsible for the DP 2 currents contributes to development of the storm-time ring current in the inner magnetosphere. This indicates that the mid-latitude ionosphere couples with the ring current region through the magnetic field lines. Using data from the Akebono satellite, Shinbori et al.[33] reported that a strong enhancement of electric field was observed in the inner magnetosphere (L = 3–6) during the main phase of a superstorm on 13 March 1989. Nishimura et al.[34] also showed that the strong electric field appeared between L = 2–6 in both dawn and dusk sectors with magnitude 2–4 $mV \cdot m^{-1}$. The maximum value appeared at L = 3 in the dusk sector during the main phase of storms, from statistical analysis of the Akebono satellite data. Kikuchi et al.[16] demonstrated that the convection electric field penetrated to the equator, intensifying the equatorial electrojet (EEJ), while the CEJ occurred at the beginning of the recovery phase. The convection electric field significantly enhanced the auroral electrojet (AEJ) at mid-latitudes (57° in corrected geomagnetic latitude or CGMLAT), while the AEJ shifted rapidly poleward toward higher latitude (67°), corresponding to occurrence of the equatorial CEJ. These observations suggest an important role of the electric field in the midlatitude ionosphere, associated with development and decay of the ring current depending on storm phase.

Direct observations of the electric field (plasma drifts) in the mid- and subauroral-latitude ionosphere during storms have been made with satellites, incoherent scatter (IS) radars, and the Super Dual Auroral Radar Network (SuperDARN)[35-38]. However, the distribution of the electric field at midlatitude has not been extensively studied, because of the limited coverage of those observations. In this work, we analyzed magnetic latitude and local time distributions of magnetic field variations on the ground for the storm event of 23–24 May 2002. This was done to clarify latitudinal and local time distributions and their storm-phase dependence of ionospheric currents, at mid-latitudes and at the daytime and nighttime equator. In the following sections, we focus on these scientific topics: (1) The contribution of ionospheric currents, asymmetric ring currents and FACs to magnetic field variations from high latitude to the magnetic equator; (2) global distribution of ionospheric equivalent currents; and (3) response of EEJs in the daytime and nighttime ionosphere. To remove the magnetic field variations caused by the magnetopause and symmetric ring current, we investigated magnetic field deviations using the SYM-H index.

2 Dataset and analysis

In this research, we used ground magnetometer data with time resolution 1 min from stations distributed between high latitudes and the magnetic equator. Coordinates of the 170 geomagnetic stations used are shown in Figure 1 by blue triangles on the world map. These datasets were obtained from the World Data Center (WDC) for Geomagnetism, Kyoto, the International Monitor for Auroral Geomagnetic Effects (IMAGE) magnetometer chain, Geophysical Institute Magnetometer Array (GIMA), Canadian Array for Realtime Investigations of Magnetic Activity (CARISMA) and NICT (National Institute of Information and Communications Technology) Space Weather Monitoring (NSWM) magnetometers[16]. Solar wind density, velocity and IMF data from the Advanced Composition Explorer (ACE) satellite were obtained through the NASA/NSSDC Coordinate Data Analysis (CDA) website. In the present data analysis, we took advantage of a metadata database search system and data analysis software[39]

of ground-based observations of the upper atmosphere, developed in the IUGONET (Inter-university Upper atmosphere Global Observation NETwork) project[40].

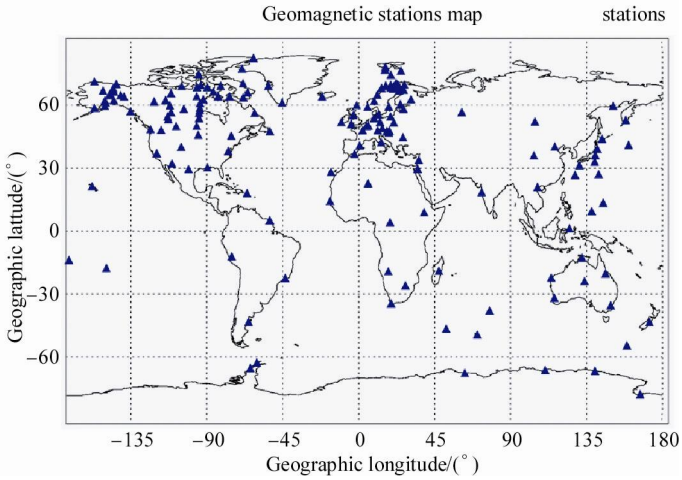

Figure 1 Map of global geomagnetic stations used in the study.

Ground magnetic field variations during geomagnetic storms are produced by ionospheric currents, FACs, ring currents, magnetopause currents and others. To derive storm-time magnetic field variations, we calculated a daily pattern of magnetic field variation from an average of 10 quiet days in one month, and subtracted the daily variation from the original magnetic field data at each magnetometer station for each day. The geomagnetic field data used are given as Cartesian components in an XYZ (north, east, vertical) geomagnetic (GM) dipole coordinate system. For identification of the 10 quiet days, we used a quiet and disturbed day list based on the *Kp* index, provided by the WDC.

3 Analysis results

3.1 Overview of geomagnetic storm on 23–24 May 2002

Panels a–f in Figure 2 show solar wind parameters (density and velocity) and three components of IMF in Geocentric Solar Magnetospheric (GSM) coordinates, measured by the ACE satellite (238, 40.0, −8.58 Re in Geocentric Solar Ecliptic (GSE) coordinates) and the SYM-H index in the period 0900–2100 on 23 May 2002. Temporal resolution of these datasets is 1 min. The solar wind and IMF data were shifted by 34 min, considering the travel time between the ACE position and earth. As shown in Figure 2, the first solar wind shock with sharp change in solar wind density from 10 to 26 proton·cc^{-1} and velocity from 425 to 591 km·s^{-1} caused the first storm sudden commencement (SSC) at 1049 UT, which shows a rapid increase of the SYM-H index. Amplitude of the SSC was 107 nT in the SYM-H index. Behind the first shock, the IMF also showed an abrupt change in all components from (−2.4, 11.0, 6.6) nT to (32.1, 46.5, 25.3) nT in the B_x, B_y and B_z components, respectively. Around 1200 UT, the IMF Bz changed from positive to negative and this persisted through 1310 UT. Around that time, the southward IMF turned completely northward. Over 114−1248 UT, the SYM-H showed a monotonic decrease to a minimum value of −93 nT at 1248 UT. This signature indicates ring current development in the inner magnetosphere, owing to the enhanced convection electric field associated with the strong southward IMF. The slight increase of SYM-H at 1248 UT was caused by northward turning of the IMF. After that, SYM-H increased to −42 nT at 1542 UT, associated with arrival of a second shock to the magnetosphere (χ = 0); it decreased again at 1545 UT after the second SSC, because of the southward IMF. After 1712 UT, SYM-H increased gradually in association with disappearance of IMF By and Bz fluctuations, although the solar wind remained at high speed (~750–800 km·s^{-1}).

3.2 Magnetic field variations from high latitudes to the magnetic equator

In this section, we examine magnetic field deviation from the SYM-H index between high latitudes and the magnetic equator to discover the contribution of ionospheric currents, asymmetric ring currents, and FACs during the geomagnetic storm. Figures 3 and 4 show magnetic field variations dX (red curves) from high latitude (first) to magnetic equator (bottom) in the American and European sectors, respectively, during the first ring current enhancement. The blue curves in each panel show the latitudinally corrected SYM-H index (SYM-H×cos λ_m, where λ_m is geomagnetic latitude at each station). The period is from 0900 to 1500 UT on 23 May 2002. The geomagnetic latitude (GMLAT) and relationship between UT and magnetic local time (MLT) are shown on the right side of each panel. In this case, the American and European sectors were located in the morning (3–9 h MLT) and noon (11–17 h MLT), respectively.

Ranges of the vertical axes are ±1 000 nT, ±200 nT and ±400 nT at high, mid-low latitudes and magnetic equator, respectively. Three vertical lines give the start time of the initial phase (A), strong enhancement (B), and weak decay (C) of the ring current in the inner magnetosphere during this magnetic storm.

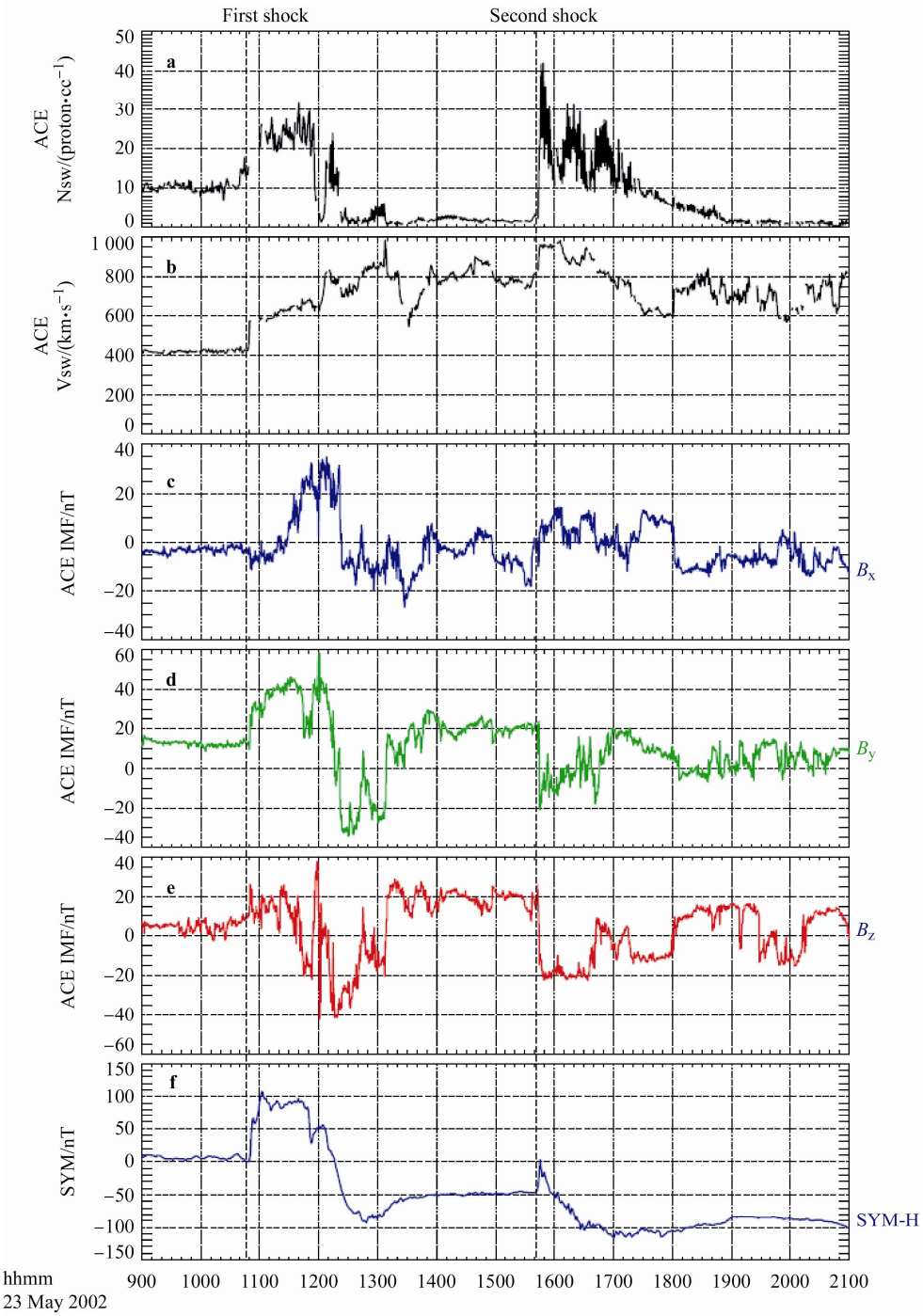

Figure 2 Overview of a geomagnetic storm event on 23–24 May 2002. **a**, Solar wind density; **b**, solar wind velocity; **c**–**e**, B_x, B_y and B_z components of interplanetary magnetic field (IMF) measured by ACE satellite at χ=238 Re in GSE coordinates; and **f**, SYM-H index from 0600 UT (23/05) to 0600 UT (24/05). Vertical dashed lines indicate arrival times of two solar wind shocks to the magnetosphere (χ=0).

The magnetic storm began at 1049 UT, in association with arrival of solar wind shock to the dayside magnetopause. In the morning sector (Figure 2), dX at the highest-latitude stations from CBB (76.44°) to YKC (68.86°) clearly showed positive deviation from the SYM-H index during the storm initial phase (1049–1148 UT), except for MEA (61.47°). A similar dX tendency was found at the mid-latitude stations from VIC (54.08°) to TUC (39.73°), and amplitude of the magnetic field deviation tended to increase with magnetic latitude. During the first enhance-

ment of the ring current as evidenced by a rapid decrease of the SYM-H index, dX at stations BLC and YKC at high latitudes increased rapidly within 10 min and decreased after 1203 UT. The same dX variation can also be seen at the highest-latitude station (CBB), but the peak value at 1200 UT is smaller than that at stations at lower latitude. The dX at MEA (61.47°) and VIC (54.08°) clearly showed negative deviation from the SYM-H index. At low latitudes (SJG and KOU) and the magnetic equator (HUA), dX showed positive deviation from that index, and the amplitude tended to increase with decreasing magnetic latitude. During the weak decay phase of the ring current indicated by a slight increase of the SYM-H index, dX at the highest-latitude station (CBB) changed from positive to negative, and recovered to the level prior to storm onset. The dX at MEA showed a gradual increase from 1223 to 1400 UT, reaching the same level of the SYM-H index. The dX at the mid-latitude stations (VIC–TUC) showed positive deviation from the SYM-H index after 1330 UT. The dX at low latitude (KOU) and the equator (HUA) changed from positive to negative with respect to the SYM-H index.

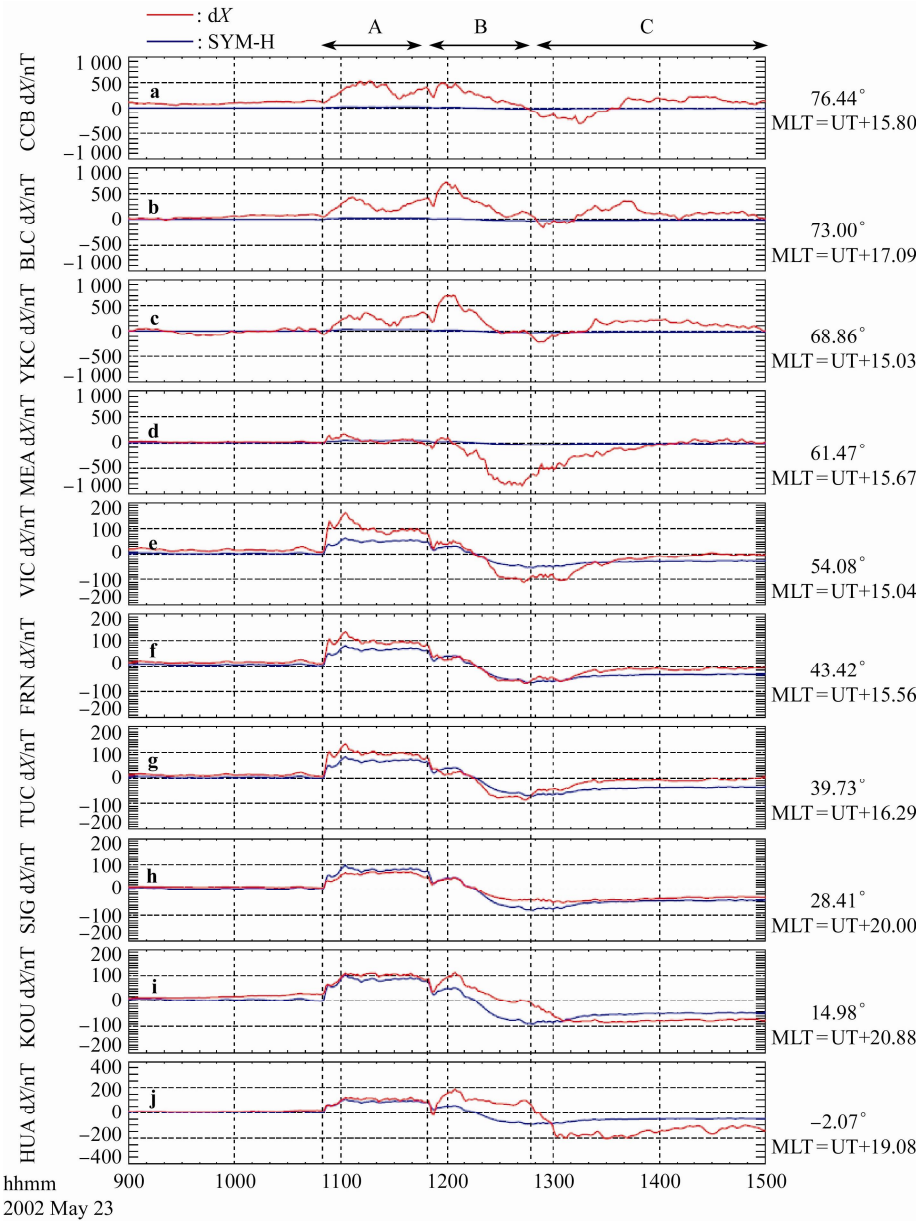

Figure 3 Magnetic field variations dX (red curves) from high latitude (first) to magnetic equator (bottom) in the American sector, during the geomagnetic storm. The blue curves in each panel show the latitudinally corrected SYM-H index (SYM-H×cosl_m, where l_m is geomagnetic latitude at each station). Geomagnetic latitude at each station is indicated at right of each panel. Three vertical dashed lines (not at hour marks) show start times of initial, first enhancement, and weak decay phases of the ring current during this storm. Periods A, B and C correspond to the above phases. The period is 0900 to 1500 UT (23/05).

In the afternoon sector (Figure 4), the magnetic field deviation from TRO (67.26°) to AAE (5.36°) was very small during the initial phase, except for HRN (73.97°). The dX at HRN showed fluctuations with large amplitude ~1 000 nT. After onset of the strong ring current enhancement, dX at the highest-latitude station (HRN) decreased significantly over ~10 min and changed from positive to negative at 1210 UT. The dX at all lower-latitude stations from TRO to EBR showed positive deviations from the SYM-H index, but the deviation at TRO and KIR became small after 1220 UT. The magnitude of magnetic field deviation from BFE to EBR tended to increase with magnetic latitude. dX variation at auroral and midlatitude stations from DOB to EBR showed an opposite sense to that in the morning (Figure 3). At the equatorial station (AAE), dX had a positive deviation after 1153 UT, but with much smaller amplitude than that at HUA in the morning. During the weak decay phase of the ring current, dX increased slightly with positive deviation at TRO and KIR, and decreased significantly at the mid-latitude stations from BFE to EBR. After 1330 UT, dX at BFE and NGK had almost the same value as the SYM-H index. At the low-latitude (EBR-QSB) and magnetic equator (AAE) stations, magnetic field deviation from the SYM-H index changed from positive to negative and magnitude tended to increase with decreasing magnetic latitude.

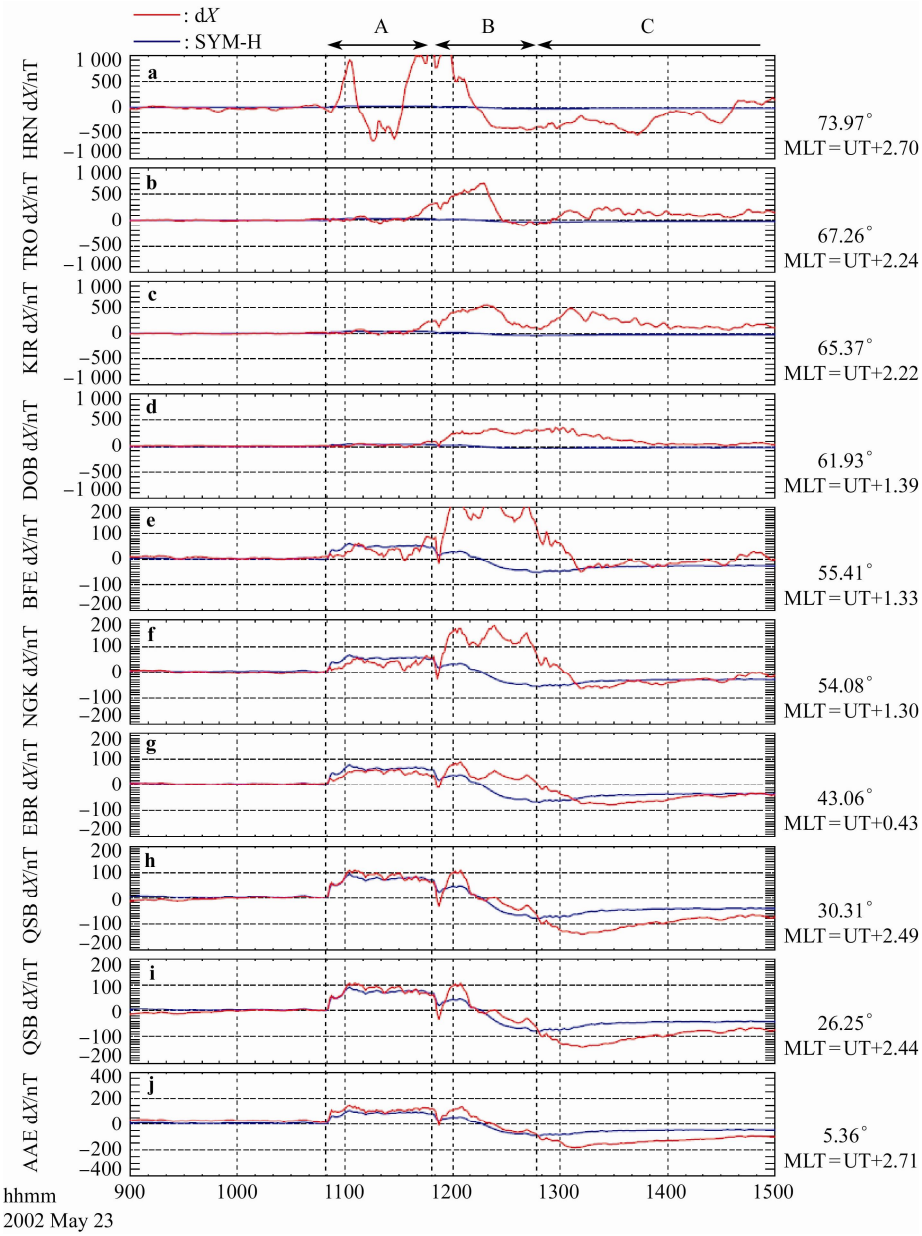

Figure 4 Magnetic field variations dX (red curves) from high latitude (first) to magnetic equator (bottom) in the European sector, during the geomagnetic storm. The blue curves in each panel show the latitudinally corrected SYM-H index (SYM-H×cosl_m, where l_m is geomagnetic latitude at each station). Geomagnetic latitude at each station is indicated at right of each panel. Three vertical dashed lines (not at hour marks) show start times of initial, first enhancement, and weak decay phases of the ring current during this storm. Periods A, B and C correspond to the above phases. The period is 0900 to 1500 UT (23/05).

Figures 5 and 6 show dX (red curves) from high latitude (second) to the magnetic equator (bottom) in the American and European sectors, respectively, during the second enhancement of the ring current. The format of this figure is the same as that of Figures 3 and 4, but the period is 1500–2100 UT on 23 May 2002. During the second enhancement of the ring current (1550–1700 UT), dX at auroral and mid-latitudes (40°–60° GMLAT) revealed negative and positive deviations from the SYM-H index in the American and European sectors, respectively. This feature was common during both the first and second enhancements of the ring current, and suggests that DP 2 type ionospheric currents are enhanced by an intensification of convection electric field associated with arrival of a southward IMF at the dayside magnetopause. Corresponding to such magnetic signatures at these latitudes, the equatorial dX at HUA increased abruptly with positive deviation from the SYM-H, and this persisted until the end of the ring current development. This signature of equatorial magnetic field perturbations indicates strong enhancement of an eastward EEJ, because of penetration of the convection electric field to the magnetic equator. However, dX at the highest-latitude stations (CBB and HRN) did not show significant variation during this period. When the SYM-H de

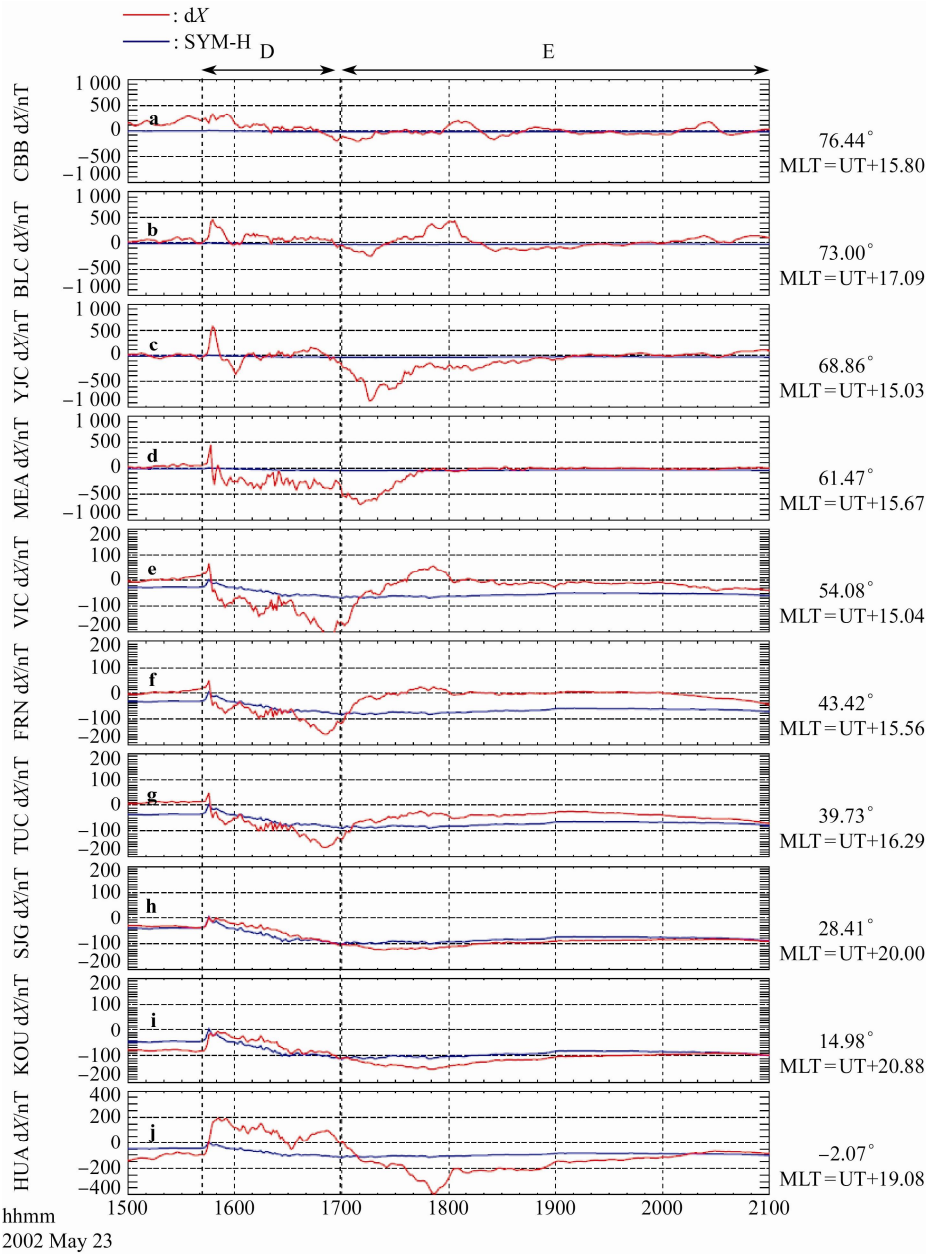

Figure 5 Magnetic field variations dX (red curves) from high latitude (first) to magnetic equator (bottom) in the American sector, during the geomagnetic storm. The blue curves in each panel show the latitudinally corrected SYM-H index (SYM-H×cosl_m, where l_m is geomagnetic latitude at each station). Geomagnetic latitude at each station is indicated at right of each panel. Three vertical dashed lines (not at hour marks) show start times of second enhancement, and weak decay phases of the ring current during this storm. Periods D and E correspond to the above phases. The period is 1500 to 2100 UT (23/05).

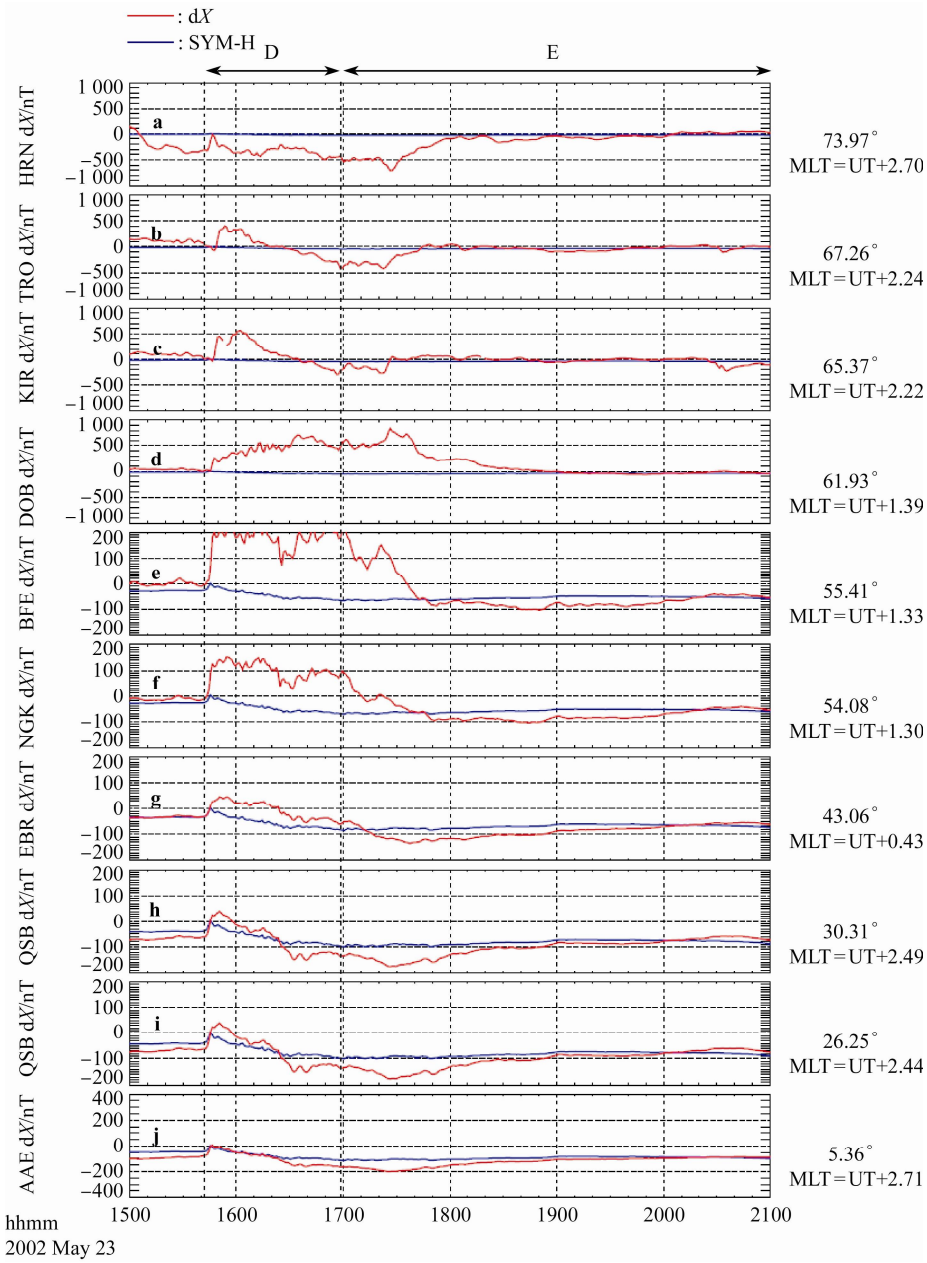

Figure 6 Magnetic field variations dX (red curves) from high latitude (first) to magnetic equator (bottom) in the European sector, during the geomagnetic storm. The blue curves in each panel show the latitudinally corrected SYM-H index (SYM-H×cosl_m, where l_m is geomagnetic latitude at each station). Geomagnetic latitude at each station is indicated at right of each panel. Three vertical dashed lines (not at hour marks) show start times of second enhancement, and weak decay phases of the ring current during this storm. Periods D and E correspond to the above phases. The period is 1500 to 2100 UT (23/05).

cline ended at 1700 UT, dX variation in auroral and mid-latitudes significantly increased and decreased in the American (11 MLT) and European (19 MLT) sectors, respectively. Equatorial dX at HUA decreased rapidly and deviation from the SYM-H index changed from positive to negative, coinciding with a dX increase at the midlatitude stations (MEA–TUC) in the morning. The minimum value of dX at HUA reached −400 nT around 1755 UT. This indicates that the direction of ionospheric currents flowing near the equator is opposite to that in mid-latitudes.

3.3 MLT distribution of magnetic field variation at mid and low latitudes

In this section, we examine storm phase dependence of MLT distributions of dX at mid and low latitudes, to reinforce the results seen in the stack plots of Figures 3–6. Figure 7 shows MLT distributions of dX at 1030 UT (panels a and b), 1220 UT (c and d), and 1320 UT (e and f) on 23 May 2002. Panels a, c and e show MLT distributions of dX at midlatitudes (35°<|GMLAT|<55°) and others at low lati-

tudes (5°<|GMLAT|<35°). Horizontal dotted red lines in each panel indicate SYM-H values at each time.

In pre-storm time (Figures 7a and 7b), d*X* at both mid and low latitudes nearly equaled the SYM-H value (6 nT), and these distributions show no MLT dependence. During enhancement of the ring current in the inner magnetosphere, MLT distributions at mid and low latitudes were different from those during pre-storm time. Figure 7c shows that dX with respect to the SYM-H value (−22 nT) at mid-latitudes was negative and positive in the morning (5–9 h MLT) and afternoon (12–18 h MLT) sectors, respectively. This local time feature is consistent with the results shown in Figures 3 and 4, which implies that the DP 2 ionospheric currents dominate the ring current effects at mid-latitudes. Conversely, d*X* in the nighttime sector showed positive deviation from the SYM-H value. This is attributable to the magnetic effect produced by enhanced R1 FACs through the Biot-Savart law.

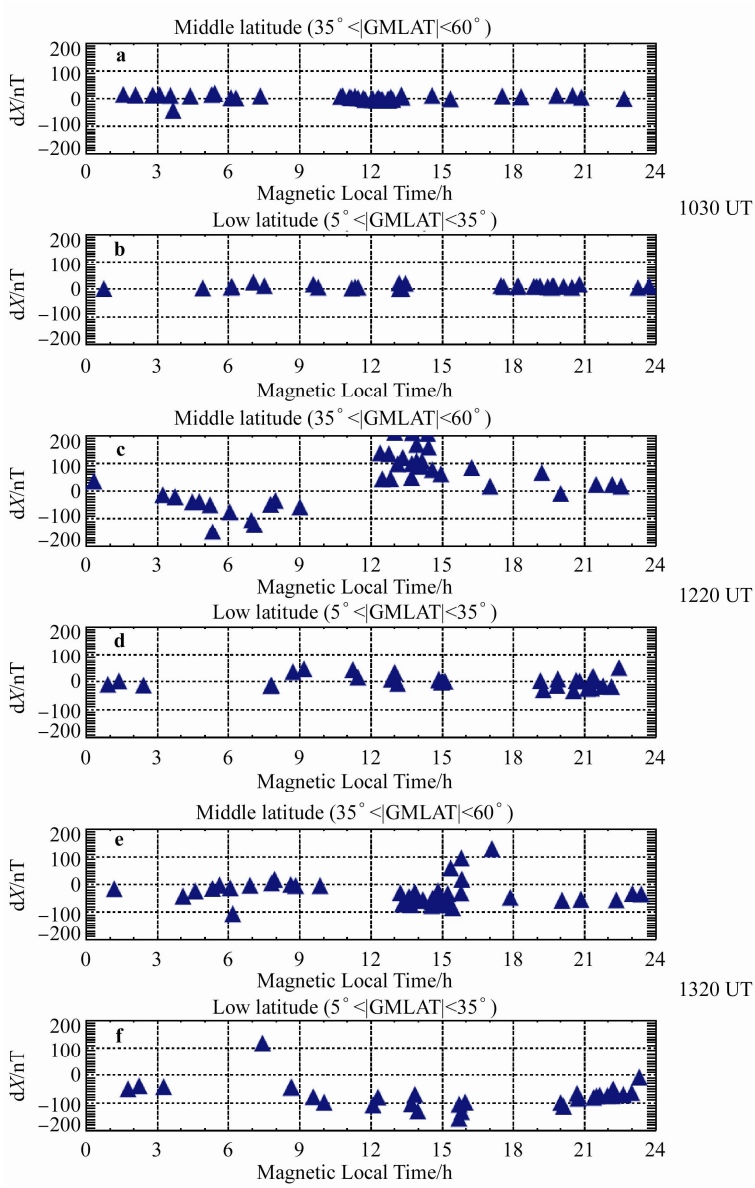

Figure 7 MLT distribution of d*X* at mid and low latitudes at 1000 UT, 1220 UT and 1320 UT on 23 May. Panels **a**, **c** and **e** show MLT distribution of d*X* at mid-latitudes (35°–60° |GMLAT|), and panels **b**, **d** and f that at low latitudes (5°–35° |GMLAT|). Horizontal dashed red lines in each panel indicate SYM-H value at each time.

At low latitudes (Figure 7d), d*X* in the dawn-noon (8–14) sector had positive deviation from the SYM-H value, whereas that in the nighttime (18−03 h MLT) sector was nearly the same as the SYM-H value (−22 nT). The maximum d*X* appeared to be located in the morning between 0900 and 1200 MLT. The MLT distribution at low latitudes was very different from that at mid-latitudes. This feature is consistent with the results shown in Figures 3 and 4. The distribution of d*X* at low latitudes does not match that of the DP 2 currents, but may be explained by magnetic effects of the

asymmetric ring current, as described by Le et al.[41]. They showed that intensity of that current has a maximum in the dusk to midnight sector and minimum in dawn to post-noon, based on magnetic field perturbations observed in the inner magnetosphere by the three magnetospheric satellites.

During the weak decay phase of the ring current associated with northward turning of the IMF (Figure 7e), dX at mid-latitudes increased in the morning (4–10 h MLT) sector and decreased in the afternoon to dusk (13–21 h MLT) sector. The MLT distribution had an opposite sense to that during the period of ring current enhancement in the inner magnetosphere. This result suggests a dominant effect of the ionospheric currents, driven by an overshielding electric field associated with the R2 FACs. However, dX in the nighttime sector approached the SYM-H value, as compared with that in panel c. This implies that the R1 FACs weaken because of northward turning of the IMF. At low latitudes, however, the MLT distribution (Figure 7f) showed that dX in the pre-noon to dusk (9–18 h MLT) sector changed from positive to negative with respect to the SYM-H value, as compared with that in Figure 7d. From this finding, it is inferred that part of the enhanced ring current region expanded to the morning sector.

3.4 Latitudinal profiles of magnetic field perturbations in the morning and afternoon sectors

In this section, we investigate whether magnetic effects of ionospheric currents are dominant at mid and low latitudes during the enhancement and weak decay phases of the ring current, comparing the latitudinally corrected SYM-H value. Figure 8 shows latitudinal distributions of dX as a function of geomagnetic latitude in pre-dawn to noon (4–12 h MLT) (panel a), noon to post-dusk (12–20 h MLT) (panel b) and nighttime (20–4 h MLT) (panel c) at 1030 UT, corresponding to the pre-storm phase. Red lines in the panels indicate the latitudinally corrected SYM-H value at each time. Blue triangles in the figure represent dX at each station. The corrected SYM-H value shows magnetic field variations from the magnetopause and symmetric ring currents at each station.

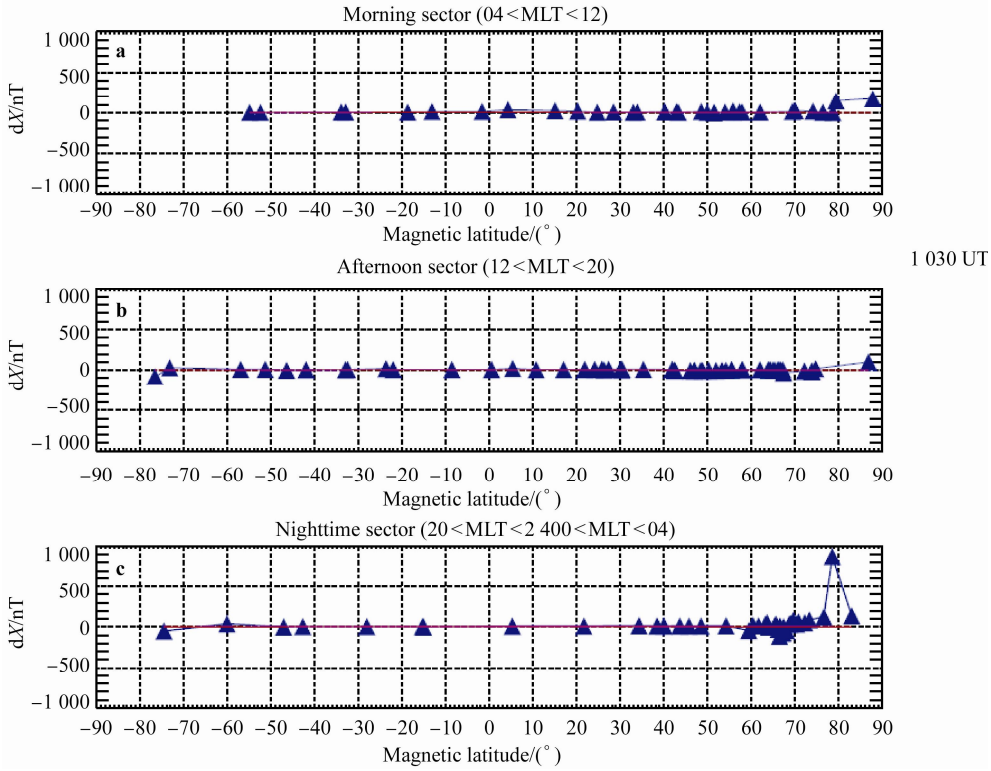

Figure 8 Latitudinal distributions of dX in the pre-dawn to noon (**a**, 4–12 h MLT), noon to post-dusk (**b**, 12–20 h MLT), and nighttime (**c**, 20–4 h MLT) at 1030 UT, corresponding to pre-storm phase. Red lines in each panel indicate the latitudinally corrected SYM-H value at each time.

During the pre-storm phase, the latitudinal dX distribution shows no latitudinal dependence in any sector, except for several higher-latitude (>75°) stations as shown in Figure 8. dX at low and mid-latitudes was close to the corrected SYM-H value. This implies that the ionospheric currents, FACs and asymmetric ring current do not develop during this phase. During the enhancement phase of the ring current at 1220 UT, the latitudinal distribution of dX in the predawn to morning sector (Figure 9a) shows negative and positive values at mid to high (40°–68°) and high (>68°) latitudes, respectively. The sign of dX changes from minus to plus is around 68°. This distribution indicates the westward and eastward ionospheric current flow at mid to high and high latitudes in the predawn to noon sector. dX at low

latitudes and the magnetic equator had a positive deviation from the corrected SYM-H value, suggesting magnetic effects of the asymmetric ring current and eastward EEJ owing to enhancement of the convection electric field in the ionosphere and magnetosphere. In the noon to post-dusk sector (Figure 9b), the latitudinal distribution of dX in the region greater than 40° shows a mirror image relationship with that in the pre-dawn to noon sector. This magnetic signature is consistent with the distribution of DP 2 ionospheric currents driven by the convection electric field carried with enhanced R1 FACs. The sign of dX changed from plus to minus around 70°. The amplitude of dX in the Southern Hemisphere tends to be smaller than that in the Northern Hemisphere. In the nighttime sector, the latitudinal distribution of dX (Figure 9c) shows negative and positive values with respect to the corrected SYM-H value in the mid to auroral (52°–65°) and high (>65°) latitudes, respectively. The dX sign changed from minus to plus around 65°, implying that the direction of ionospheric currents turns from westward to eastward. The turning point is at the lowest latitude, relative to that in the morning and afternoon sectors. During the weak decay phase of the ring current associated with northward turning of the IMF, the latitudinal dX distribution shows slight increase and decrease in the mid-latitudes between 40° and 58° in the morning and afternoon sectors, as shown in Figures 10a and 10b. The dX distribution at auroral latitudes (58°–75°) showed latitudinal dependence during the enhancement phase of the ring current, but another change point of dX appeared at higher latitude, around 80°. However, dX at low latitudes (<20° |GMLAT|) of the afternoon sector had a negative deviation with respect to the corrected SYM-H value compared with that in the morning sector, except for the magnetic equator. This MLT distribution of low-latitude dX was nearly consistent with the result obtained from Figure 7. A negative deviation of equatorial dX with large amplitude of 200 nT in the morning sector (Figure 10a) indicates the magnetic effect of the westward EEJ driven by a dusk-to-dawn electric field, accompanied by the R2 FACs. In contrast, the latitudinal dX distribution at low and mid-latitudes (<50° |GMLAT|) of the nighttime sector (Figure 10c) shows no clear dependence on magnetic latitude, and deviation from the corrected SYM-H value is not evident.

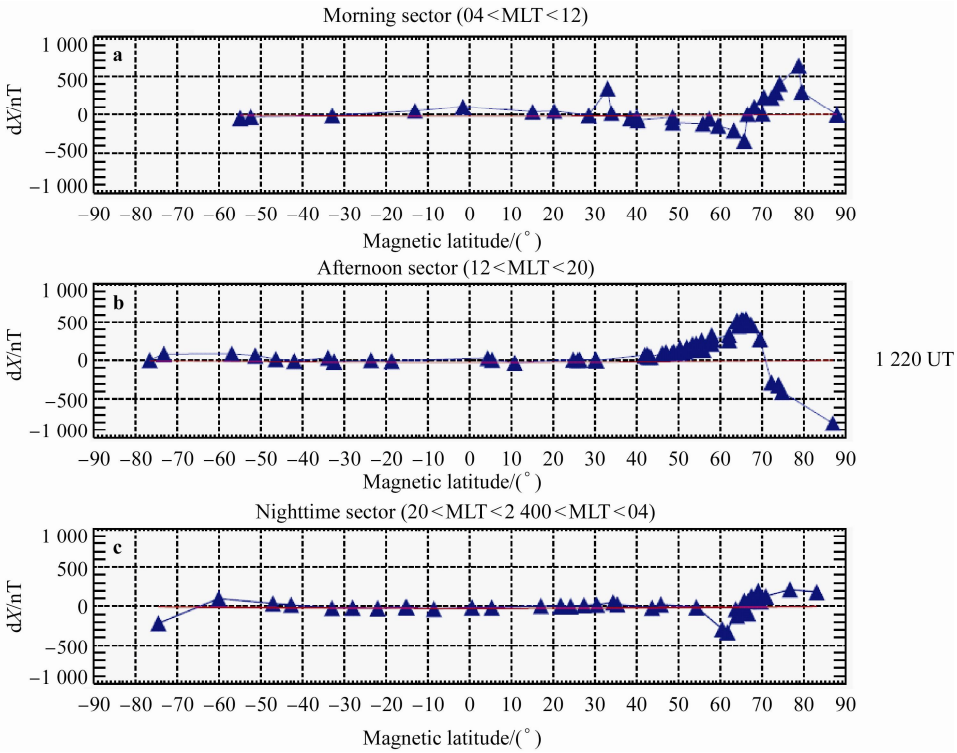

Figure 9 Latitudinal distributions of dX in the pre-dawn to noon (**a**, 4–12 h MLT), noon to post-dusk (**b**, 12–20 h MLT), and nighttime (**c**, 20–4 h MLT) at 1220 UT, corresponding to enhancement phase of the ring current. Red lines in each panel indicate the latitudinally corrected SYM-H value at each time.

3.5 Distribution of ionospheric equivalent currents during the geomagnetic storm

In this section, we derive the global distribution of ionospheric equivalent currents from magnetic field deviations dX and dY at each station, to examine temporal and spatial variations of global ionospheric currents during the geomagnetic storms. We found that the magnetic field variation of dX at low latitudes is mainly caused by the magnetic

effect of asymmetric ring and magnetopause currents from the results of magnetic latitude and local time dependence shown in Figures 7–10. Therefore, we subtracted the north-south component of disturbed magnetic field (dX_low) at low-latitude ($5 \leqslant |\lambda_m| < 35$) stations from the north-south component at each one to minimize the asymmetric ring and magnetopause currents. Considering the local time dependence of the magnetopause and ring current effects reported by Araki et al.[42] and Tsuji et al.[17], we used geomagnetic field data at four low-latitude stations (Bangui (BNG), Hachijo (HTY), Honolulu (HON), and Kourou (KOU)) as a reference field for the subtraction of geomagnetic field data at other stations in the four sectors $0 \leqslant$ MLT<6, $6 \leqslant$ MLT<12, $12 \leqslant$ MLT<18 and $18 \leqslant$ MLT<24, respectively. We also added the latitudinal correction (dX_low×cos λ_m) to the low-latitude magnetic field data. The parameter λ_m in units of degrees represents the magnetic latitude of each magnetometer station.

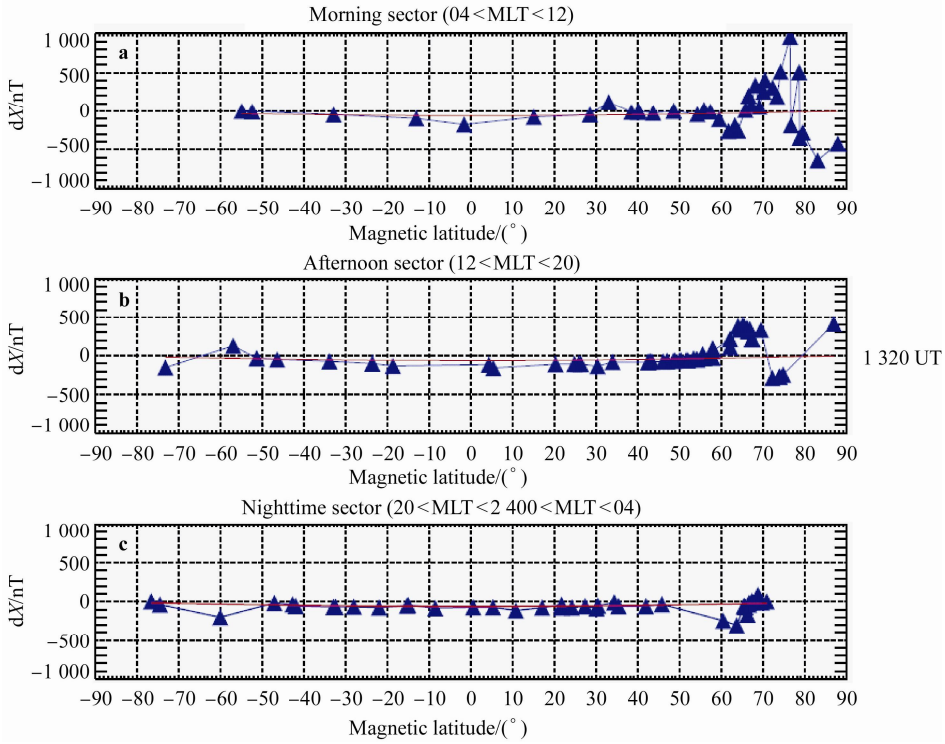

Figure 10 Latitudinal distributions of dX in the pre-dawn to noon (**a**, 4–12 h MLT), noon to post-dusk (**b**, 12–20 h MLT), and nighttime (**c**, 20–4 h MLT) at 1320 UT, corresponding to weak decay phase of the ring current. Red lines in each panel indicate the latitudinally corrected SYM-H value at each time.

Figure 11 shows the SYM-H index from 0800 UT on 23 May to 0800 UT on 24 May, along with six world maps depicting equivalent current vectors in the Northern Hemisphere at 1030 and 1130 UT on 23 May. Red circles on the maps indicate the geomagnetic stations. The geomagnetic coordinate is used for the observation points and unit vectors of ionospheric equivalent currents drawn on the maps. The four values outside each map are magnetic local time. As shown in Figure 11a, the ionospheric equivalent currents during the pre-storm phase were directed westward from 67° to 20° in the European sector (11–12 h MLT). In the American sector (0–2 h MLT), the direction of the equivalent currents varied by station, but a clockwise vortex can be seen in the high-latitude region from 75° to 65° around 1–2 h (MLT). The center of the vortex seems to correspond to the footprint of downward FACs. Equivalent currents at mid and low latitudes (30°–60°) of the nighttime (23–03 h MLT) sector are directed eastward. This signature can be interpreted as the magnetic effect of the downward FACs, obeying the Biot–Savart law. During the first enhancement phase of the ring current (Figure 11b), the equivalent current vectors in the American sector (4–8 h MLT) showed the clockwise vortex centered near 70° and 4 h (MLT). This current vortex expanded to a low-latitude region ~30°. In the European sector (14 h MLT), the current vectors were directed westward in the high-latitude region greater than 65°, and turned eastward in the auroral and mid-latitude regions from 65° to 42°. This current distribution shows an opposite sense to that in the American sector. From the distribution of ionospheric equivalent current vectors, it is suggested that the R1 FACs and related ionospheric currents were significantly enhanced by the arrival of southward IMF to the dayside magnetosphere. In Figure 12a corresponding to the weak decay phase of the ring current associated with northward turning of the IMF, the clockwise current vortex disappears and the two anti-clockwise vortices appear at mid-latitudes (40°–60°) and polar cap (70°–80°) of the dawn sector (4–8 h MLT). Moreover, the direction of the current vectors changed from eastward to westward around 65° and 6 h MLT. The distribution of cur-

rent directions at mid to high latitudes (>45°) of the European sector (15–16 h MLT) did not show clear change compared with that in the American sector, but the current direction at mid to low latitudes was directed equatorward or westward. In Figure 12b corresponding to the period of nearly constant SYM-H value (Figure 2), the current vectors show almost a westward direction at many stations of the American sector. The vectors in the European sector (55°–75°) showed almost the same pattern as that in Figure 12a. In Figure 13a corresponding to the second enhance-

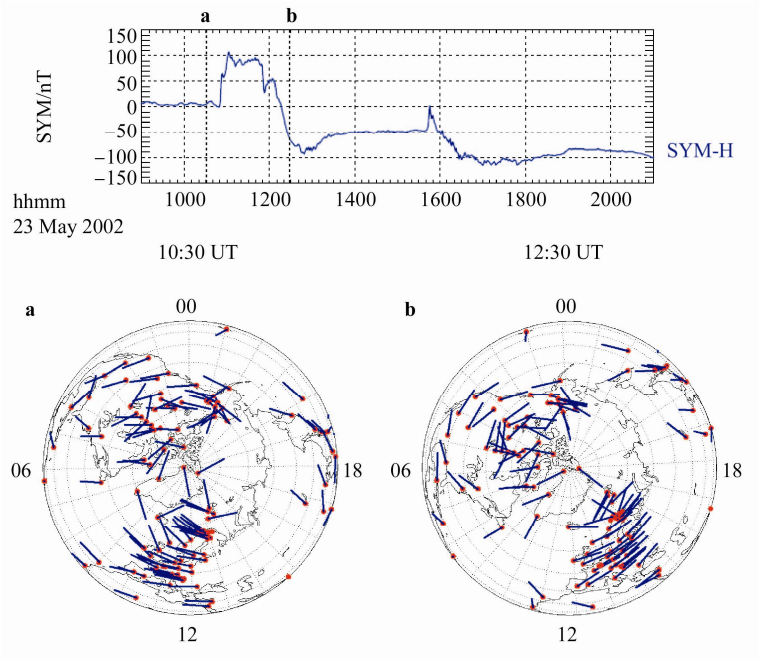

Figure 11 SYM-H index in the period 0800 UT (23/05) to 0800 UT (24/05), and two world maps depicting equivalent current vectors in the Northern Hemisphere at 1030 and 1130 UT on 23 May. Red circles on the maps indicate geomagnetic stations. The geomagnetic coordinate is used for the observation points and current vectors on the maps.

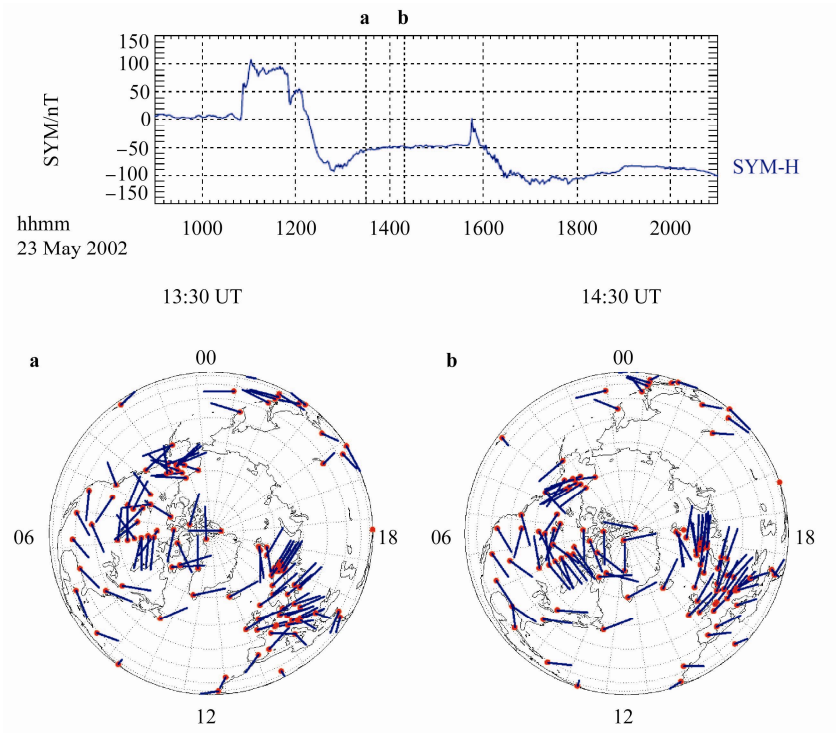

Figure 12 SYM-H index in the period 0800 UT (23/05) to 0800 UT (24/05), and two world maps depicting equivalent current vectors in the Northern Hemisphere at 1330 and 1430 UT on 23 May. Red circles on the maps indicate geomagnetic stations. The geomagnetic coordinate is used for the observation points and current vectors on the maps.

ment of the ring current, the global distribution of current vectors indicated nearly the same pattern as that in Figure 11b. This suggests that the R1 FACs and related ionospheric currents intensify significantly across a wide region from high to low latitudes, during the two enhancement phases of the ring current associated with southward turning of the IMF. In Figure 13b corresponding to the period of nearly constant SYM-H value, current vectors in the American sector (10–14 h MLT) had various directions at each station. The vectors in the auroral region of ~65° (6–12 h MLT) were directed westward. Moreover, the clockwise current vortex appeared in the polar cap region (70°–85°) near the noon. However, the direction of current vectors in the European sector (19–22 h MLT) turned from westward to eastward around 70°, and from eastward to westward or southward around 60°.

3.6 Comparison between daytime and nighttime equatorial magnetic field variations

Figure 14 shows the SYM-H index and magnetic field variations of the dX component at the daytime and nighttime magnetic equator, HUA-HON (second), and YAP-HTY (third). The period is 0900 to 2100 UT on 23 May 2002, and includes the two geomagnetic storm events. At almost the same time as the SSC onset (1049 UT) of the first geomagnetic storm, dX at the nighttime equator (YAP) showed an abrupt decrease of 40 nT within a few minutes. A negative dX persisted until the end of the main phase. dX at the daytime equator (HUA) increased by 20 nT after the SSC onset and its amplitude was more enhanced during the main phase. The dX amplitude in the nighttime was larger than that in the nighttime during the initial phase. dX at the daytime and nighttime equator changed from positive to negative and from negative to positive, respectively, within 10–20 min after initiation of the recovery phase. These magnetic field variations indicate that the ionospheric currents near the magnetic equator flow eastward and westward in the daytime and nighttime, respectively. Judging from the magnetic field variations of dX, intensity of the equatorial current in the nighttime is smaller than that in the daytime. For the second geomagnetic storm event, the magnetic field variation of dX showed the same pattern during the main and recovery phases. Since station HUA was located near the noon in this case, the amplitude of the magnetic field variation was more enhanced relative to that during the first geomagnetic storm. The dX peak amplitude at HUA reached 200 nT at 1550 UT after SSC onset (1545 UT). This value was seven times larger than that at YAP.

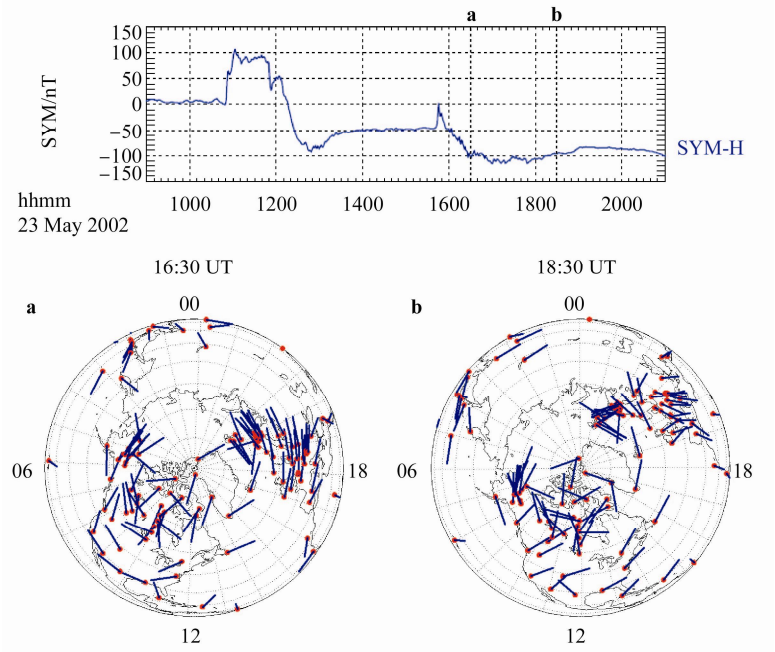

Figure 13 SYM-H index in the period 0800 UT (23/05) to 0800 UT (24/05), and two world maps depicting equivalent current vectors in the Northern Hemisphere at 1630 and 1830 UT on 23 May. Red circles on the maps indicate geomagnetic stations. The geomagnetic coordinate is used for the observation points and current vectors on the maps.

4 Discussion

4.1 Penetration of storm-time electric field to the equatorial ionosphere

The large-scale convection electric field strengthens significantly owing to the magnetic reconnection process at the dayside magnetopause, associated with arrival of a strong southward IMF to the magnetosphere. The enhanced convection electric field develops the ring current in the inner magnetosphere. Magnetic field intensity at low latitudes decreased significantly under the influence of

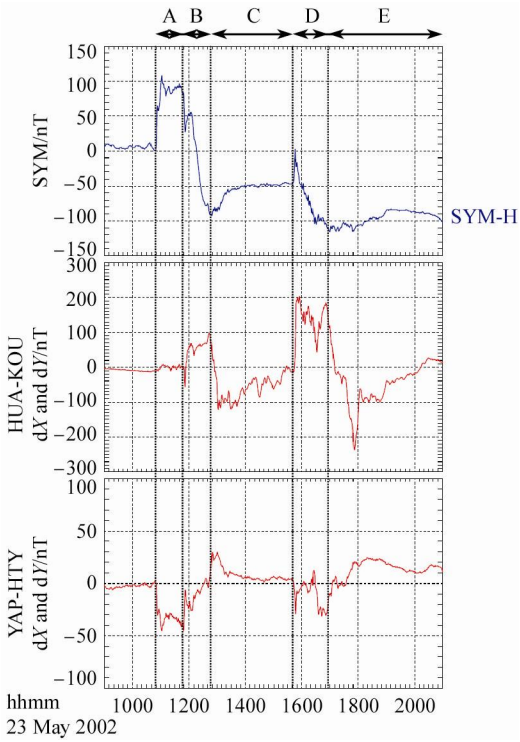

Figure 14 SYM-H index and equatorial magnetic field variations d*X* at HUA and YAP during the two geomagnetic storms. In this case, HUA and YAP were located on the dayside and nightside, respectively. Periods A, B, and C correspond to the initial phase after SSC, first enhancement, and weak decay phases of the ring current, respectively. D and E correspond to the second enhancement and decay. The period is 0900 to 2100 UT on 23 May.

magnetic field perturbations produced by the enhanced ring current, which characterizes geomagnetic storm phenomena. It is well-known that the enhanced storm-time convection electric field penetrates from high latitude to the magnetic equator[16,43-44] and causes the DP 2 currents at mid-latitudes during the storm main phase[17]. Based on geomagnetic field analysis, Tsuji et al.[17] showed that the influence of ionospheric currents on magnetic field variations reached mid-latitude regions (~30°) during the main phase of a geomagnetic storm. In the geomagnetic storm event analyzed in the present study, the eastward and westward currents appeared at mid-latitudes (~30°) of the morning and afternoon sectors, respectively, during the main phase. The direction of these currents changed around 70° (morning) and 65° (afternoon) (Figure 11b). These magnetic signatures indicate that the footprint of the R1 FACs was located at these latitudes and that the convection electric field responsible for those FACs penetrates to mid-latitudes ~30°. Based on observations by DMSP satellites, Heelis and Mohapatra[45] reported that during superstorms (Dst<−300 nT), electron precipitation and threshold boundaries of ionospheric zonal drift velocity at 1800 h MLT moved to the lower latitude region (20°–45°). They showed that the auroral oval expands to 45° and the convection electric field penetrates to at least 20° during these storms. This tendency is consistent with expansion of the DP 2 currents to mid-latitudes and equatorward movement of the AEJ as shown in Figure 11. The electric field associated with the DP 2 currents should be observed at the magnetic equator by incoherent scatter radar[43-44] and satellite[46]. The equatorward expansion of the ionospheric currents would lead to penetration of the convection electric field deep into the inner magnetosphere, as has been observed by several satellites[33-34,47-48].

The large-scale convection electric field decreased rapidly just before the beginning of the geomagnetic storm recovery phase, owing to northward turning or weakening of the southward component of the IMF (Figure 2). At that time, ionospheric currents were reversed at mid-latitudes (30°–50°) of the American sector (Figure 12a) and westward/eastward EEJs were dominant at the dayside/nightside equator (Figure 14). This implies that the R2 FAC system is more dominant than that of the R2 FAC at mid-latitude and the magnetic equator. This situation has been called overshielding[16]. As shown in Figure 12a, eastward currents in the morning sector reversed to westward around 50°–60° during the recovery phase of the geomagnetic storm. From this result, the R2 FAC footprint is located at mid-latitudes of 50°–60°, which coincides with the magnetic field line of L = 3.0–4.0 in the inner magnetosphere. Therefore, it is inferred that the origin of the R2 FACs is in the inner magnetosphere of L = 3.0–4.0, where the ring current flows westward. The reversal of the EEJ associated with sudden decrease of the convection electric field has been reported in several works[16-17]; however, the present study clarifies that the response of magnetic field variation to northward turning or weakening of the southward component of the IMF varies between the American and European sectors. The direction of ionospheric currents did not change from eastward to westward at mid-latitudes of the European sector (Figure 12a). This problem of variable response of the R2 FACs will be addressed in a future study.

4.2 Asymmetric ring current as observed at low latitudes

In Section 3.4, we showed dawn-dusk asymmetry of the MLT distribution of d*X* observed at low latitudes during development of the ring current in the inner magnetosphere (Figures 7d and 7f). while the asymmetry was not observed during the pre-storm phase (Figure 7b). The ring current simulations[49-50] and satellite[51-52] and ground magnetometer[17,53] observations of the ring current showed that the ring current is strongly asymmetric during the main phase and becomes symmetric during the recovery phase with good correlation to the intensification and weakening of the convection electric field. The present study showed that the MLT distribution of magnetic field perturbations in low latitudes (Figure 7d and 7f) represents the asymmetric feature during the enhancement and early decay phases of the ring current. This result is consistent with the simulation[54] and direct measurement[51]. The asymmetry of the ring cur-

rent could be associated with overshielding during the early decay phases, which leads to a rapid enhancement of the eastward EEJ.

Yu et al.[55] made comprehensive studies of magnetic field perturbations on the ground at low, mid and high latitudes, based on ground magnetometer observations and global magnetohydrodynamics (MHD) simulation. Using MHD model BATSRUS (Block-Adaptive Tree Solar wind Roe Upwind Scheme) coupled with an inner magnetospheric model (Rice Convection Model[56]), they calculated magnetic field variations produced by the ionospheric Hall and Pederson currents, FACs, and magnetospheric currents (ring, tail and magnetopause). Their result showed that the northward component of magnetic field variations at low latitudes was mostly caused by magnetospheric currents dominated by the ring current; the dawn-dusk asymmetry at low and mid-latitudes was caused by the ring current, and the FACs caused the day-night asymmetry. The present result is consistent with that shown by Yu et al.[55].

4.3 Nighttime equatorial electrojet

The present study reveals that the westward/eastward ionospheric currents flowed in the nighttime equatorial ionosphere during the main/recovery phase of the geomagnetic storms, corresponding to the eastward/westward electrojet in the daytime. This result indicates that the convection and overshielding electric fields penetrate to the magnetic equator in the nighttime and drive the westward electrojet, owing to the Cowling effect. Tsuji et al.[17] also reported that the nighttime westward electrojet tended to strengthen with significant amplitude during the storm period. Peak amplitude reached 35 nT in the nighttime and 270 nT in the daytime during the main phase of the geomagnetic storm on 7 September 2002. Abdu et al.[57] estimated the nighttime E-layer Cowling conductivity at 0.2 times the daytime conductivity, based on magnetic disturbances at the daytime and nighttime magnetic equator during magnetic storms. Shinbori et al.[9] calculated magnetic field variations in the H component at the equator with the potential solver of Tsunomura[58], obtaining the amplitude ratio 0.14 between nighttime (0230 LT) and daytime (1230 LT) ionospheric currents. In the present results (Figure 12), at 1655 UT during the main phase, the ratio 0.22 was obtained from YAP-HTY dX (~0155 LT at YAP) divided by HUA-KOU dX (~1155 LT at HUA). This ratio is in good agreement with those of Abdu et al.[57]. From the above discussion, the penetrating electric fields cause significant magnetic effects at the magnetic equator, even under nighttime ionospheric conditions.

4.4 FAC effects on magnetic field variations at mid and low latitudes

The magnetic field disturbance observed on the ground is a superposition of magnetic effects of ionospheric and magnetospheric (magnetopause, ring, tail and field-aligned) currents. The R1 FACs flowing into and out of the polar ionosphere in the morning and evening produce negative and positive variations of magnetic field dX on the dayside and nightside, according to the Biot-Savart effects. These variations correspond to the ionospheric equivalent currents directed westward and eastward in the noon and night, respectively. As shown in Figure 11b, the direction of the ionospheric equivalent currents was almost eastward in the Japanese sector located in the nighttime (~21 h MLT). Since intensity of ionospheric currents flowing in the nighttime is very weak because of low ionospheric conductivity, magnetic field disturbances in the nighttime mid and low latitudes are mainly from the magnetic effects of FACs. Shinbori et al.[9] verified that this effect is dominant in the nighttime from the result of Tsunomura's model[49]. Therefore, from the above discussion, it is concluded that the nighttime equivalent current derived from magnetic field variations does not actually correspond to ionospheric currents. Similar positive magnetic variations in the nighttime have been observed during sudden commencements (SCs), substorms, and storms[9,17,59-63]. Araki et al.[63] found the nighttime enhancement of SC amplitude at mid-latitude, based on statistical results of magnetic field data obtained from several stations in the Japanese sector. They concluded that magnetic phenomena during SCs were because of the magnetic effect of the R1 type of FACs generated during the main impulse. Using long-term geomagnetic field data with time resolution 1 s, Shinbori et al.[10] demonstrated seasonal variation of the magnetic disturbances, owing to FAC effects. It is believed that such seasonal dependence of nighttime magnetic field variations also appears at mid and low latitudes during a storm period. Verification of this seasonal effect will be done in future work.

4.5 NBZ FAC contribution to magnetic field variations in the polar cap during the geomagnetic storm recovery phase

The northward IMF causes high-latitude reconnection tailward of the earth's cusp between the magnetic fields in the magnetosheath and magnetopause[64-67], and enhances sunward ionospheric convection in the dayside polar cap because of a dusk-to-dawn electric field carried by a pair of upward and downward (FAC) systems[68-73]. These FACs are known as the NBZ current system. The upward (downward) NBZ currents produce counterclockwise (clockwise) ionospheric currents around prenoon (postnoon) in the polar cap. Dayside reverse two-cell convection is commonly observed at the noon-midnight meridian, under the northward IMF condition[74-75]. For the present storm event, the ionospheric equivalent currents showed that the counterclockwise cell appeared in the polar cap (~80°) of the prenoon (10–11 h MLT) during the recovery phase (Figures 11c, 11d and 11f), when the IMF was directed northward. Appearance of the NBZ FAC system in the polar cap is consistent with Erickson et al.[75]. They showed four-cell convection during the recovery phase of the 9 November 2004 superstorm, based on integrated SuperDARN data analysis. In

Figure 11d, the AEJ (60°–70°) was completely directed eastward, and the clockwise convection cell related to R1 FACs disappeared at auroral latitudes. The direction of the ionospheric currents corresponds with the ionospheric NBZ current cell equatorward of the dawnside FAC footprint. The contribution of a dusk-to-dawn electric field associated with the NBZ current system to the equatorial counter electrojet will be verified in a subsequent study.

5 Conclusion

Temporal and spatial evolution of worldwide geomagnetic field variations during two geomagnetic storms of 23–24 May 2002 were investigated using geomagnetic field data with time resolution of 1 min. These data were acquired from the CARISMA, GIMA, IMAGE, MACCS and NSWM networks, and the WDC for Geomagnetism of Kyoto University. The daytime ionospheric equivalent current during the storm main phase showed that twin-vortex ionospheric currents driven by R1 FACs intensified significantly and expanded to the low-latitude region less than 30° (GMLAT). Centers of the twin-vortex ionospheric currents were around 70° and 65° in the morning and afternoon, respectively. Corresponding to the intensification of the R1 FACs, there was enhancement of the eastward/westward EEJ at the daytime/nighttime dip equator. This signature suggests that the enhanced convection electric field penetrates both the daytime and nighttime equator. In the nighttime mid to low latitudes, the direction of the equivalent current was northward. This implies that the nighttime magnetic field disturbances originate from the magnetic effect of the R1 FACs. However, during the recovery phase associated with strong northward turning of the IMF, the daytime equivalent current showed that two new pairs of twin vortices, which were different from two-cell ionospheric currents driven by the R1 FACs, appeared in the polar cap and at mid-latitude. The vortex in the polar cap led to the enhanced NBZ FACs driven by the lobe reconnection tailward of the cusps, owing to the northward IMF, whereas the vortex in mid-latitude was generated by enhanced R2 FACs connected to the asymmetric ring current flowing westward in the inner magnetosphere. Associated with these magnetic field variations at mid-latitudes and the polar cap, the equatorial magnetic field variation showed a strongly negative signature. This was produced by a westward EEJ current owing to the dusk-to-dawn electric field.

Acknowledgments This work was supported by the Inter-university Upper atmosphere Global Observation NETwork (IUGONET) project, funded by the Ministry of Education, Culture, Sports, Science and Technology (MEXT), Japan, the National Institute of Polar Research through General Collaboration Projects (Grant no. 23-14), and JSPS KAKENHI (Grant no. 11020535). We used geomagnetic field data obtained from the CARISMA, GIMA, IMAGE, MACCS and NSWM networks, and the ASY/SYM index provided by WDC for Geomagnetism, Kyoto. We acknowledge A. Lazarus, A. Szabo and R. P. Lepping for the IMF-8 solar wind and MAG data, L. Frank and S. Kokubun for the Geotail CPI and MGF data, D. J. McComas and N. F. Ness for the ACE SWEPAM and MAG data, and R. Lin and R. Lepping for the Wind 3DP and MFI data provided through CDAWeb.

References

1 Nishida A, Iwasaki N, Nagata T. The origin of fluctuations in the equatorial electrojet: A new type of geomagnetic variation. Ann Geophys, 1966, 22: 478-484.

2 Nishida A. Coherence of geomagnetic DP2 magnetic fluctuations with interplanetary magnetic variations. J Geophys Res, 1968, 73(17): 5549-5559, doi: 10.1029/JA073i017p05549.

3 Kikuchi T, Lühr H, Kitamura T, et al. Direct penetration of the polar electric field to the equator during a DP2 event as detected by the auroral and equatorial magnetometer chains and the EISCAT radar. J Geophys Res, 1996, 101(A8): 17161-17173, doi: 10.1029/96JA01299.

4 Kikuchi T, Araki T, Maeda H, et al. Transmission of polar electric fields to the equator. Nature, 1978, 273(5664): 650-651, doi: 10.1038/273650a0.

5 Kikuchi T, Araki T. Horizontal transmission of the polar electric field to the equator. J Atmos Terr Phys, 1979, 41(9): 927-936, doi: 10.1016/0021-9169(79)90094-1.

6 Hirono M. A theory of diurnal magnetic variations in equatorial regions and conductivity of the ionosphere E region. J Geomag Geoelectr, 1952, 4(1): 7-21, doi: 10.5636/jgg.4.7.

7 Baker W G, Martyn D F. Electric currents in the ionosphere. I. The conductivity, Phil Trans R Soc London A, 1953, 246(913): 281-294, doi: 10.1098/rsta.1953.0016.

8 Araki T. A physical model of the geomagnetic sudden commencement// Solar Wind Sources of Magnetospheric Ultra-Low-Frequency Waves. Washington, D. C.: AGU, 1994: 183-200.

9 Shinbori A, Tsuji Y, Kikuchi T, et al. Magnetic latitude and local time dependence of the amplitude of geomagnetic sudden commencements. J Geophys Res, 2009, 114(A4): A04217, doi: 10.1029/2008JA013871.

10 Shinbori A, Tsuji Y, Kikuchi T, et al. Magnetic local time and latitude dependence of amplitude of the main impulse (MI) of geomagnetic sudden commencements and its seasonal variation. J Geophys Res, 2012, 117(A8): A08322, doi: 10.1029/2012JA018006.

11 Motoba T, Kikuchi T, Lühr H, et al. Global Pc5 caused by a DP 2-type ionospheric current system. J Geophys Res, 2002, 107(A2): SMP 8-1-SMP 8-12, doi: 10.1029/2001JA900156.

12 Nishida A, Kamide Y. Magnetospheric processes preceding the onset of an isolated substorm: A case study of the March 31, 1978, substorm. J Geophys Res, 1983, 88(A9): 7005-7014, doi: 10.1029/JA088iA09p07005.

13 Kikuchi T, Pinnock M, Rodger A, et al. Global evolution of a substorm-associated DP2 current system observed by SuperDARN and magnetometers. Adv Space Res, 2000, 26(1): 121-124, doi: 10.1016/S0273-1177(99)01037-6.

14 Kikuchi T, Lühr H, Schlegel K, et al. Penetration of auroral electric fields to the equator during a substorm. J Geophys Res, 2000, 105(A10): 23251-23261, doi: 10.1029/2000JA900016.

15 Wilson G R, Burke W J, Maynard N C, et al. Global electrodynamics observed during the initial and main phases of the July 1991 magnetic storm. J Geophys Res, 2001, 106(A11): 24517-24539, doi: 10.1029/2000JA 000348.

16 Kikuchi T, Hashimoto K K, Nozaki K. Penetration of magnetospheric electric fields to the equator during a geomagnetic storm. J Geophys Res, 2008, 113(A6): A06214, doi: 10.1029/2007JA012628.

17 Tsuji Y, Shinbori A, kikuchi T, et al. Magnetic latitude and local time distributions of ionospheric currents during a geomagnetic storm. J Geophys Res, 2012, 117(A7): A07318, doi: 10.1029/2012JA017566.

18 Vasyliunas V M. Mathematical models of magnetospheric convection and its coupling to the ionosphere // Particles and Fields in the Magnetosphere. Hingham, MA: D. Reidel. Pub. Co., 1970: 60-71.

19 Vasyliunas V M. The interrelationship of magnetospheric processes // Earth's Magnetospheric Processes. Norwell, MA: D. Reidel. Pub. Co., 1972: 29-38.

20 Jaggi R K, Wolf R A. Self-consistent calculation of the motion of a sheet of ions in the magnetosphere. J Geophys Res, 1973, 78(16): 2852-2866, doi: 10.1029/JA078i016p02852.

21 Southwood D J. The role of hot plasma in magnetospheric convection. J Geophys Res, 1977, 82(35): 5512-5520, doi: 10.1029/JA082i035p05512.

22 Senior C, Blanc M. On the control of magnetospheric convection by the spatial distribution of ionospheric conductivities. J Geophys Res, 1984, 89(A1): 261-284, doi: 10.1029/JA089iA01p00261.

23 Somayajulu V V, Reddy C A, Viswanathan K S. Penetration of magnetospheric convective electric field to the equatorial ionosphere during the substorm of March 22, 1979. Geophys Res Lett, 1987, 14(8): 876-879, doi: 10.1029/GL014i008p00876.

24 Peymirat C, Richmond A D, Kobea A T. Electrodynamic coupling of high and low latitudes: Simulations of shielding/overshielding effects. J Geophys Res, 2000, 105(A10): 22991-23003, doi: 10.1029/2000JA000057.

25 Rastogi R G, Patel V L. Effect of interplanetary magnetic field on ionosphere over the magnetic equator. Proc Indiana Acad Sci, 1975, 82(4): 121-141.

26 Kelley M C, Fejer B G, Gonzales C A. An explanation for anomalous equatorial ionospheric electric fields associated with a northward turning of the interplanetary magnetic field. Geophys Res Lett, 1979, 6(4): 301-304, doi: 10.1029/GL006i004p00301.

27 Fejer B G, Gonzales C A, Farley D T, et al. Equatorial electric fields during magnetically disturbed conditions 1. The effect of the interplanetary magnetic field. J Geophys Res, 1979, 84(A10): 5797-5802, doi: 10.1029/JA084iA10p05797.

28 Gonzales C A, Kelley M C, Fejer B G, et al. Equatorial electric fields during magnetically disturbed conditions 2. Implications of simultaneous auroral and equatorial measurements. J Geophys Res, 1979, 84(A10): 5803-5812, doi: 10.1029/JA084iA10p05803.

29 Rastogi R G. Geomagnetic storms and electric fields in the equatorial ionosphere. Nature, 1977, 268(5619): 422-424, doi: 10.1038/268422a0.

30 Rastogi R G. Midday reversal of equatorial ionospheric electric field. Ann Geophys, 1997, 15(10): 1309-1315, doi: 10.1007/s00585-997-1309-2.

31 Kikuchi T, Hashimoto K K, Kitamura T I, et al. Equatorial counterelectrojets during substorms. J Geophys Res, 2003, 108(A11): 1406, doi: 10.1029/2003JA009915.

32 De Zeeuw D L, Sazykin S, Wolf R A, et al. Coupling of a global MHD code and an inner magnetospheric model: Initial results. J Geophys Res, 2004, 109(A12): A12219, doi: 10.1029/2003JA010366.

33 Shinbori A, Nishimura Y, Ono T, et al. Electrodynamics in the duskside inner magnetosphere and plasmasphere during a super magnetic storm on March 13-15, 1989. Earth Planets Space, 2005, 57(7): 643-659.

34 Nishimura Y, Shinbori A, Ono T, et al. Storm-time electric field distribution in the inner magnetosphere. Geophys Res Lett, 2006 33(22): L22102, doi: 10.1029/2006GL027510.

35 Yeh H-C, Foster J C, Rich F J, et al. Storm time electric field penetration observed at mid-latitude. J Geophys Res, 1991, 96(A4): 5707-5721, doi: 10.1029/90JA02751.

36 Foster J C, Rich F J. Prompt midlatitude electric field effects during severe geomagnetic storms. J Geophys Res, 1998, 103(A11): 26367-26372, doi: 10.1029/97JA03057.

37 Baker J B H, Greenwald R A, Ruohoniemi J M, et al. Observations of ionospheric convection from the Wallops SuperDARN radar at middle latitudes. J Geophys Res, 2007, 112(A1): A01303, doi: 10.1029/2006JA011982.

38 Kikuchi T, Ebihara Y, Hashimoto K K, et al. Penetration of the convection and overshielding electric fields to the equatorial ionosphere during a quasiperiodic DP 2 geomagnetic fluctuation event. J Geophys Res, 2010, 115(A5): A05209, doi: 10.1029/2008JA013948.

39 Tanaka Y, Shinbori A, Hori T, et al. Analysis software for the upper atmosphere data developed by the IUGONET project and its application to the polar science. Adv Polar Sci, 2013, 24(4): 231-240.

40 Hayashi H, Koyama Y, Hori T, et al. Inter-university upper atmosphere global observation network (IUGONET). Data Sci J, 2013, 12: WDS179.

41 Le G, Russell C T, Takahashi K. Morphology of the ring current derived from magnetic field observations. Ann Geophys, 2004, 22(4): 1267-1295, doi: 10.5194/angeo-22-1267-2004.

42 Araki T, Funato K, Iguchi T, et al. Direct detection of solar wind dynamic pressure effect on ground geomagnetic field. Geophys Res Lett, 1993, 20(9): 775-778, doi: 10.1029/93GL00852.

43 Huang C-S, Foster J C, Kelley M C. Long-duration penetration of the interplanetary electric field to the low-latitude ionosphere during the main phase of magnetic storms. J Geophys Res, 2005, 110(A11): A11309, doi: 10.1029/2005JA011202.

44 Fejer B G, Jensen J W, Kikuchi T, et al. Equatorial ionospheric electric fields during the November 2004 magnetic storm. J Geophys Res, 2007, 112(A10): A10304, doi: 10.1029/2007JA012376.

45 Heelis R A, Mohapatra S. Storm time signatures of the ionospheric zonal ion drift at middle latitudes. J Geophys Res, 2009, 114(A2): A02305, doi: 10.1029/2008JA013620.

46 Huang C S. Continuous penetration of the interplanetary electric field to the equatorial ionosphere over eight hours during intense geomagnetic storms. J Geophys Res, 2008, 113(A11): A11305, doi: 10.1029/2008JA013588.

47 Burke W J, Maynard N C, Hagan M P, et al. Electrodynamics of the inner magnetosphere observed in the dusk sector by CRRES and DMSP during the magnetic storm of June 4-6, 1991. J Geophys Res, 1998, 103(A12): 29399-29418, doi: 10.1029/98JA02197.

48 Wygant J, Rowland D, Singer H J, et al. Experimental evidence on the role of the large spatial scale electric field in creating the ring current. J Geophys Res, 1998, 103(A12): 29527-29544, doi: 10.1029/98JA01436.

49 Ebihara Y, Ejiri M. Simulation study on fundamental properties of the storm-time ring current. J Geophys Res, 2000, 105(A7): 15843-15859, doi: 10.1029/1999JA900493.

50 Ebihara Y, Ejiri M. Numerical simulation of the ring current: Review. Space Sci Rev, 2003, 105(1-2): 377-452, doi: 10.1023/A:1023905607888.

51 Terada N, Iyemori T, Nosé M, et al. Storm-time magnetic field variations observed by the ETS-VI satellite. Earth Planet Space, 1998, 50: 853-864.

52 Ebihara Y, Ejiri M, Nilsson H, et al. Statistical distribution of the storm-time proton ring current: POLAR measurements. Geophys Res Lett, 29(20): 30-1-30-4, doi: 10.1029/2002GL015430.

53 Hashimoto K K, Kikuchi T, Ebihara Y. Response of the magnetospheric convection to sudden interplanetary magnetic field changes as deduced from the evolution of partial ring currents. J Geophys Res, 2002, 107(A11): SMP 1-1-SMP 1-14, doi: 10.1029/2001JA009228.

54 Liemohn M W, Kozyra J U, Thomsen M F, et al. Dominant role of the asymmetric ring current in producing the stormtime Dst. J Geophys Res, 2001, 106(A6): 10883-10904, doi: 10.1029/2000JA000326.

55 Yu Y Q, Ridley A J, Welling D T, et al. Including gap region field-aligned currents and magnetospheric currents in the MHD calculation of ground-based magnetic field perturbations. J Geophys Res, 2010, 115(A8): A08207, doi: 10.1029/2009JA014869.

56 Wolf R A, Harel M, Spiro R W, et al. Computer simulation of inner magnetospheric dynamics for the magnetic storm of July 29, 1977. J Geophys Res, 1982, 87(A8): 5949-5962, doi: 10.1029/JA087iA08p05949.

57 Abdu M A, Maruyama T, Batista I S, et al. Ionospheric responses to the October 2003 superstorm: Longitude/local time effects over equatorial low and middle latitudes. J Geophys Res, 2007, 112(A10): A10306, doi: 10.1029/2006JA012228.

58 Tsunomura S. Numerical analysis of global ionospheric current system

including the effect of equatorial enhancement. Ann Geophys, 1999, 17(5): 692-706, doi: 10.1007/s00585-999-0692-2.

59 Kamide Y, Yasuhara F, Akasofu S I. On the cause of northward magnetic field along the negative X axis during magnetospheric substorms. Planet Space Sci, 1974, 22(8): 1219-1229, doi: 10.1016/0032-0633(74)90006-3.

60 Reddy C A, Kumar S A, Somayajulu V V. An observational test for the ionospheric or magnetospheric origin of night-time geomagnetic positive bays at low and mid-latitudes. Planet Space Sci, 1988, 36(11): 1149-1154, doi: 10.1016/0032-0633(88)90069-4.

61 Kikuchi T, Tsunomura S, Hashimoto K, et al. Field-aligned current effects on midlatitude geomagnetic sudden commencements. J Geophys Res, 2001, 106(A8): 15555-15565, doi: 10.1029/2001JA900030.

62 Sastri J H. Penetration electric fields at the nightside dip equator associated with the main impulse of the storm sudden commencement of 8 July 1991. J Geophys Res, 2002, 107(A12): SIA 9-1-SIA 9-8, doi: 10.1029/2002JA009453.

63 Araki T, Keika K, Kamei T, et al. Nighttime enhancement of the amplitude of geomagnetic sudden commencements and its dependence on IMF-B_z. Earth Planets Space, 2006, 58(1): 45-50.

64 Dungey J W. The structure of the exosphere, or adventures in velocity space//DeWitt C, Hieblot J, LeBeau L. Geophysics: The earth's environment. New York: Gordon and Breach, 1963: 503-550.

65 Song P, Russell C T. Model of the formation of the low-latitude boundary layer for strongly northward interplanetary magnetic field. J Geophys Res, 1992, 97(A2): 1411-1420.

66 Phan T, Frey H U, Frey S, et al. Simultaneous Cluster and IMAGE observations of cusp reconnection and auroral proton spot for northward IMF. Geophys Res Lett, 2003, 30(10): 1509, doi: 10.1029/2003GL016885.

67 Trattner K J, Fuselier S A, Petrinec S M. Location of the reconnection line for northward interplanetary magnetic field. J Geophys Res, 2004, 109(A3): A03219, doi: 10.1029/2003JA009975.

68 Iijima T, Potemra T A, Zanetti L J, et al. Large-scale Birkeland currents in the dayside polar region during strongly northward IMF: A new Birkeland current system. J Geophys Res, 1984, 89(A9): 7441-7452.

69 Zanetti L J, Potemra T A, Iijima T, et al. Ionospheric and Birkeland current distributions for northward interplanetary magnetic field: Inferred polar convection. J Geophys Res, 1984, 89(A9): 7453-7458.

70 Iijima T, Shibaji T. Global characteristics of northward IMF-associated (NBZ) field-aligned currents. J Geophys Res, 1987, 92(A3): 2408-2424.

71 Cowley S W H. Magnetosphere-ionosphere interactions: A tutorial review //Magnetospheric current systems. Washington D.C.: AGU, 2000: 91-106.

72 Iijima T, Fujii R, Hesse M, et al. Field-aligned currents in geospace: Substance and significance//Magnetospheric current systems. Washington D.C.: AGU, 2000: 107-129.

73 Maezawa K. Magnetospheric convection induced by the positive and negative Z components of the interplanetary magnetic field: Quantitative analysis using polar cap magnetic records. J Geophys Res, 1976, 81(3): 2289-2303.

74 Burch J L, Reiff P H, Menietti J D, et al. IMF B_y-dependent plasma flow and Birkeland currents in the dayside magnetosphere: 1. Dynamics Explorer observations. J Geophys Res, 1985, 90(A2): 1577-1593.

75 Erickson, Goncharenko L P, Nicolls M J, et al. Dynamics of north American sector ionospheric and thermospheric response during the November 2004 superstorm. J Atmos Solar-Terr Phys, 2010, 72(4): 292-301, doi: 10.1016/j.jastp.2009.04.001.